Equilibrium Calculation of Gaseous Reactive Systems with Simultaneous Species Adsorption

Mingheng Li *

Abstract

This work focuses on the calculation of chemical equilibrium in a gaseous reactive system with simultaneous single or multiple species adsorption under isothermal and isobaric conditions. Two different algorithms are developed following the minimization of Gibbs free energy and the concept of equilibrium constant, respectively. In either case the problem formulation is converted to a set of nonlinear algebraic equations solved using the Newton-Raphson scheme. An example of steam reforming of ethanol with simultaneous CO_2 adsorption is used to illustrate the proposed approaches. It is shown that at $T = 500$ °C and $P = 5$ bar, the CO_2 removal ratio should exceed 40% in order to achieve a decent enhancement in hydrogen production and purity. An integrated process that combines the endothermic reforming and the exothermic combustion of CH_4 from the off-gas supplemented with simultaneous CO_2 adsorption in the reforming process yields a theoretical maximum overall conversion rate of 86.3% (the corresponding H_2 purity out of the reformer is 89.4% on wet basis or 96.2% on dry basis) with little or no external heat supply. The analysis in this work is potentially useful in the design and optimization of adsorption enhanced reforming reactors for hydrogen generation and other applicable reactive systems.

Keywords: Equilibrium, Adsorption, Optimization, Hydrogen, Adsorption Enhanced Reforming

1 Introduction

Chemical equilibrium in a reactive system is a state where the chemical activity of each species does not have a net change over time.[1] The calculation of chemical equilibrium provides the thermodynamic limit of a chemical process and has been traditionally used in the design and analysis of chemical equipment such as turbines and engines etc.[2,3] The advances in chemical equilibrium algorithms have been significantly facilitated by the ever-increasing computational power of modern computers. One milestone in chemical equilibrium calculation is the development of the NASA chemical equilibrium and applications (CEA) code, which is capable of tracking hundreds of species in a gaseous reactive system and has been used in various applications such as rockets, incident/reflected shocks and Chapman-Jouguet detonations etc.[4] The so-called Gibbs reactor module that is based on the minimization of Gibbs free energy has also been incorporated in various modern engineering solvers including Pro/II®

---

[*] Department of Chemical and Materials Engineering, California State Polytechnic University, Pomona, CA 91768 USA. Tel: +1-909-869-3668. Fax: +1-909-869-6920. E-mail: minghengli@csupomona.edu.

and Aspen Hysys® to predict equilibrium compositions.[5,6] Nowadays thermodynamic analyses based on chemical equilibrium calculations have been found in a variety of applications such as material interfacial phenomena,[7,8] biological processes,[9,10] and reacting nozzle flows[11–14] to name a few.

More recently, researchers in various groups have shown a great interest in the application of chemical equilibrium to processes related to hydrogen generation and fuel cells.[15–23] As reducing the demand on fossil resources has been a public concern, hydrogen, being a potential carrier of clean energy, is now an important topic that may lead into a new era of energy research. The generation of hydrogen can be realized through various routes such as steam reforming of hydrocarbons,[24] gasification of coal,[25] chemical looping combustion of coal,[26] water splitting by thermochemical cycle[27] and electrolytic decomposition of water[28] etc. In particular, hydrogen generation from biomass has caught lots of attention as it is a potentially viable, renewable and carbon-neutral (or even carbon-negative in conjunction with sequestration) process.[29] Most of these processes involve water gas shift reaction ($CO + H_2O = CO_2 + H_2$). If CO_2 can be simultaneously removed as the water gas shift reaction proceeds, the thermodynamic limitation can be circumvented and therefore, the chemical equilibrium shifts to the right, resulting in an enhancement in the extent of the forward reaction and the hydrogen yield.

This work focuses on the development of computational algorithms for chemical equilibrium calculations in gaseous reactive systems with simultaneous single or multiple species adsorption. The algorithms are then applied to the thermodynamic analysis of steam reforming of ethanol. Implications to an integrated autothermal process for hydrogen generation from steam reforming of hydrocarbons are discussed at the end of this work.

2 Chemical equilibrium calculation through nonlinear optimization

For a closed system under constant temperature and pressure, the Gibbs free energy decreases as equilibrium is approached. Therefore, one approach to equilibrium calculation in an isothermal and isobaric reactive system is to minimize its total Gibbs free energy. The mathematical formulation generally leads to a nonlinear optimization problem which can be solved using numerical methods. This approach is advantageous over the equilibrium constant method when simultaneously tracking a large number of species is necessary because it circumvents specifying a set of reactions a priori. To this end, it is worth noting that even though the NASA CEA package is capable of handling various types of equilibrium calculations, no species adsorption is explicitly accounted for in the current code.[4]

The focus of this work is to calculate the chemical equilibrium of a reactive gaseous system with species adsorption, which is a common problem to adsorption enhanced reactive systems.[30–35] In the problem formulation, the following assumptions are made: (1) the reactive system is maintained at isothermal and isobaric conditions; (2) the gaseous phase obeys the ideal gas law; (3) there is no heterogeneous reaction on the surface of the adsorbent; and (4) there is no condensed species in the entire reactive system. Consider such a reactive system with one kilogram of reactants, the Gibbs free energy (G) of the entire reactive system is:

$$G = \sum_{j=1}^{s}(\mu_j^{(g)} n_j^{(g)} + \mu_j^{(ads)} n_j^{(ads)}) \tag{1}$$

where s is the total number of species, n_j is the amount of species j in mole, μ is the chemical potential, and the superscripts $^{(g)}$ and $^{(ads)}$ stand for properties related to species in the gas phase and on the surface, respectively. When equilibrium is reached, the following criteria should be satisfied:

$$\mu_j^{(ads)} = \mu_j^{(g)} \quad (j = 1, ..., s) \tag{2}$$

For a gaseous species that obeys ideal gas law, its chemical potential can be calculated using the following equation:[1]

$$\mu_j^{(g)} = \mu_j^{0(g)} + RT \ln \frac{P}{P^0} + RT \ln \frac{n_j^{(g)}}{n_T^{(g)}} \quad (j = 1, ..., s) \tag{3}$$

where T and P are temperature and pressure of the system, respectively, R is the gas constant (8.314 J/mol/K), ^{0} stands for properties under standard conditions ($P^0 = 1$ bar), and $n_T^{(g)} = \sum_{j=1}^{s} n_j^{(g)}$. A detailed expression for $\mu_j^{(ads)}$ might not be necessary because the relationship between the gaseous species and the adsorbed species can sometimes be experimentally obtained. Based on the Langmuir isotherm widely used in the analysis of adsorption phenomena[36] or experimental observations (e.g., equilibrium chemisorption isotherms of CO_2 on hydrotalcites[18,35]), the adsorption/desorption equilibrium typically follows the relationship below:

$$n_j^{(ads)} = S \frac{n_{j,sat}^{(ads)} \beta_j P_j}{1 + \sum_{j=1}^{s} \beta_j P_j} = S \frac{n_{j,sat}^{(ads)} \beta_j \frac{n_j^{(g)}}{n_T^{(g)}} P}{1 + \sum_{j=1}^{s} \beta_j \frac{n_j^{(g)}}{n_T^{(g)}} P} \quad (j = 1, ..., s) \tag{4}$$

where $n_j^{(ads)}$ is the actual adsorbed amount of species j in mole, $n_{j,sat}^{(ads)}$ is the saturated surface concentration in mole/m^2, S is the total surface area of the adsorbent, β_j is a constant for species j under isothermal conditions, P_j is the partial pressure of species j in the gas phase. Based on Eq. 4, the ratio of $n_j^{(ads)}$ to $n_j^{(g)}$ is expressed as follows:

$$r_j = \frac{n_j^{(ads)}}{n_j^{(g)}} = \frac{S n_{j,sat}^{(ads)} \beta_j P}{n_T^{(g)} + \sum_{j=1}^{s} \beta_j n_j^{(g)} P} \quad (j = 1, ..., s) \tag{5}$$

There are two ways to solve the relationship between the equilibrium composition and the amount of adsorbent. One could start with the surface area of the adsorbent and include Eq. 4 in the optimization problem to solve the equilibrium composition. Alternatively, one could start with r_j and solve the equilibrium composition from the optimization problem. The surface area of the adsorbent is then calculated based on Eq. 5 and the equilibrium composition. The latter approach is used in this work because the number of constraints can be significantly reduced in the optimization problem. However, it is important to note that r_j are not independent if multiple species are adsorbed simultaneously. In such a case, r_j should be specified based on the following relationship:

$$\frac{r_i}{r_j} = \frac{n_{i,sat}^{(ads)}\beta_i}{n_{j,sat}^{(ads)}\beta_j} \tag{6}$$

To minimize the Gibbs free energy of the entire system described by Eq. 1, the mass balance should be satisfied at the same time. This is achieved by the so-called atomic balance equations.[37] Let a_{ij} be the number of chemical element i contained in species j, the atomic balance equation is:

$$\sum_{j=1}^{s} a_{ij} n_j^{(g)} + \sum_{j=1}^{s} a_{ij} n_j^{(ads)} = \sum_{j=1}^{s} a_{ij} n_j^{(g)}(0) \quad (i = 1, ..., \epsilon) \tag{7}$$

where ϵ is the total number of chemical elements in this reactive system. $b_i(0) = \sum_{j=1}^{s} a_{ij} n_j^{(g)}(0)$ is the number of moles of elements i per kilogram reactants. It is worth noting that the effective number of equations in Eq. 7 is equal to the rank of the atomic matrix, which might be less than ϵ occasionally. In such a case, Eq. 7 should be replaced by its minimum realization. Interested readers are directed to open literature for more details.[37] However, the optimization algorithms can still be developed in a similar manner.

Based on the above analysis, the calculation of equilibrium compositions is formulated as the following nonlinear optimization problem:

$$\begin{aligned}
\min_{n_j^{(g)}, n_j^{(ads)}} G &= \sum_{j=1}^{s} (\mu_j^{(g)} n_j^{(g)} + \mu_j^{(ads)} n_j^{(ads)}) \\
s.t. & \\
0 &= \sum_{j=1}^{s} a_{ij} n_j^{(g)} + \sum_{j=1}^{s} a_{ij} n_j^{(ads)} - b_i(0) \quad (i = 1, ..., \epsilon) \\
\mu_j^{(ads)} &= \mu_j^{(g)} \quad (j = 1, ..., s) \\
\frac{n_j^{(ads)}}{n_j^{(g)}} &= r_j \quad (j = 1, ..., s) \\
\mu_j^{(g)} &= \mu_j^{0(g)} + RT \ln \frac{P}{P^0} + RT \ln \frac{n_j^{(g)}}{n_T^{(g)}} \quad (j = 1, ..., s) \\
n_T^{(g)} &= \sum_{j=1}^{s} n_j^{(g)}
\end{aligned} \tag{8}$$

Eq. 8 can be simplified by canceling the terms related to the adsorbed species. The resulting problem is:

$$\begin{aligned}
\min_{n_j^{(g)}} G &= \sum_{j=1}^{s}(1+r_j)\mu_j^{(g)} n_j^{(g)} \\
s.t. & \\
0 &= \sum_{j=1}^{s}(1+r_j)a_{ij}n_j^{(g)} - b_i(0) \quad (i=1,...,\epsilon) \\
\mu_j^{(g)} &= \mu_j^{0(g)} + RT\ln\frac{P}{P^0} + RT\ln\frac{n_j^{(g)}}{n_T^{(g)}} \quad (j=1,...,s) \\
n_T^{(g)} &= \sum_{j=1}^{s} n_j^{(g)}
\end{aligned} \tag{9}$$

Strictly speaking, inequity constraints $n_j \geq 0$ $(j=1,...,s)$ should be included in the optimization problem described by Eq. 8 or 9. This is handled by solving $\ln n_j$ instead of n_j in the detailed solution procedure[4] . Even when this strategy is applied, sometimes n_j can still be very close (or theoretically equal) to zero during the iterations and singularity problems occur when taking logarithms of extremely small positive numbers. These can be avoided by purposely setting the minimum of n_j to a very small number (e.g., 10^{-100}). During the iterations, any n_j that is smaller than its minimum will be replaced by this lower limit. Such a modification does not have an effect on the accuracy of the solution because the contribution of $n_j\mu_j$ of these components to the total Gibbs free energy would be very close to zero (Note that $\lim_{n_j\to 0} n_j \ln n_j = -\lim_{n_j\to 0} n_j = 0$ based on L'Hopital's rule). With this in mind, the optimization problem described in Eq. 9 is then converted to a set of nonlinear algebraic equations using the lagrange multiplier method. First we define $f = \sum_{j=1}^{s}(1+r_j)\mu_j^{(g)}n_j^{(g)} + \sum_{i=1}^{\epsilon}\lambda_i\left[\sum_{j=1}^{s}(1+r_j)a_{ij}n_j^{(g)} - b_i(0)\right]$, where λ_i are the lagrange multipliers, the optimal solution to the optimization problem of Eq. 9 should be determined by solving the following nonlinear algebraic equations:

$$\begin{aligned}
0 &= \frac{\partial f}{\partial n_j^{(g)}} = (1+r_j)\mu_j^{(g)} + \sum_{i=1}^{\epsilon}(1+r_j)a_{ij}\lambda_i \quad (j=1,...,s) \\
0 &= \frac{\partial f}{\partial \lambda_i} = \sum_{j=1}^{s}(1+r_j)a_{ij}n_j^{(g)} - b_i(0) \quad (i=1,...,\epsilon) \\
\mu_j^{(g)} &= \mu_j^{0(g)} + RT\ln\frac{P}{P^0} + RT\ln\frac{n_j^{(g)}}{n_T^{(g)}} \quad (j=1,...,s) \\
n_T^{(g)} &= \sum_{j=1}^{s} n_j^{(g)}
\end{aligned} \tag{10}$$

The variables to be determined are $n_j^{(g)}$ $(j=1,...,s)$, λ_i $(i=1,...,\epsilon)$ and $n_T^{(g)}$. These $s+\epsilon+1$ variables in Eq. 10 can be solved using the decent Newton-Raphson method. The central idea of the Newton-Raphon method is to apply multi-variable Taylor series expansion to a nonlinear vector function and then use truncated terms that contain only the first order derivatives to build a linear iterative formula. The formula can be then used to compute the solution with a given initial guess close to the solution; interested readers may refer to specialized books[38] for details. Following a method employed by the NASA CEA package,[4] the iterative variables are chosen to be $\Delta \ln n_j^{(g)}$ $(j = 1, ..., s)$, $\Delta \ln n_T^{(g)}$ and $\pi_i = -\lambda_i/RT$ $(i = 1, ..., \epsilon)$ in order to avoid taking the logarithm of negative numbers in the iteration procedure. Note here $\pi_i = -\lambda_i/RT$ is solved directly at each iteration step.

With the definition of π_i, the first equation in Eq. 10 can be converted to a dimensionless form as follows:

$$(1 + r_j)\frac{\mu_j^{(g)}}{RT} - \sum_{i=1}^{\epsilon}(1 + r_j)a_{ij}\pi_i \quad = \quad 0 \quad (j = 1, ..., s) \tag{11}$$

which has the following Newton-Raphson iterative formula:

$$\frac{(1 + r_j)\mu_j^{(g)}}{RT} - \sum_{i=1}^{\epsilon}(1 + r_j)a_{ij}\pi_i - \frac{\partial\left[\frac{(1 + r_j)\mu_j^{(g)}}{RT}\right]}{\partial \ln n_T}\Delta \ln n_T^{(g)} + \frac{\partial\left[\frac{(1 + r_j)\mu_j^{(g)}}{RT}\right]}{\partial \ln n_j}\Delta \ln n_j^{(g)} \quad = \quad 0 \quad (j = 1, ..., s) \tag{12}$$

or

$$\Delta \ln n_j^{(g)} \quad = \quad -\frac{\mu_j^{(g)}}{RT} + \sum_{i=1}^{\epsilon} a_{ij}\pi_i + \Delta \ln n_T^{(g)} \quad (j = 1, ..., s) \tag{13}$$

Similarly, the Newton-Raphson iterative formulas for the other equations can be determined as follows:

$$\sum_{j=1}^{s}(1 + r_j)a_{ij}n_j^{(g)} - \sum_{j=1}^{s}a_{ij}n_j^{(g)}(0) + \sum_{j=1}^{s}(1 + r_j)a_{ij}n_j^{(g)}\Delta \ln n_j^{(g)} \quad = \quad 0 \quad (i = 1, ..., \epsilon) \tag{14}$$

and

$$\sum_{j=1}^{s}n_j^{(g)} - n_T^{(g)} + \sum_{j=1}^{s}n_j^{(g)}\Delta \ln n_j^{(g)} - n_T^{(g)}\Delta \ln n_T^{(g)} \quad = \quad 0 \tag{15}$$

In order to expedite the calculation, especially when a large number of species are present in the reactive system, the so-called "reduced Gibbs iteration" scheme has been proposed to significantly reduce the number of variables in the iteration steps.[4] The idea is to cancel $\Delta \ln n_j^{(g)}$ in Eqs. 14 and 15 using Eq. 13. Consequently, Eqs. 14 and 15 are converted to

$$\begin{aligned}&\sum_{k=1}^{\epsilon}\left[\sum_{j=1}^{s}(1 + r_j)a_{kj}a_{ij}n_j^{(g)}\right]\pi_k + \left[\sum_{j=1}^{s}(1 + r_j)a_{ij}n_j^{(g)}\right]\Delta \ln n_T^{(g)} \\ =\quad &\left[\sum_{j=1}^{s}a_{ij}n_j^{(g)}(0) - \sum_{j=1}^{s}(1 + r_j)a_{ij}n_j^{(g)} + \sum_{j=1}^{s}(1 + r_j)a_{ij}n_j^{(g)}\frac{\mu_j^{(g)}}{RT}\right] \quad (i = 1, ..., \epsilon)\end{aligned} \tag{16}$$

and

$$\sum_{k=1}^{\epsilon}\left[\sum_{j=1}^{s}a_{kj}n_j^{(g)}\right]\pi_k + \left[\sum_{j=1}^{s}n_j^{(g)} - n_T^{(g)}\right]\Delta \ln n_T^{(g)} \quad = \quad \left[n_T^{(g)} - \sum_{j=1}^{s}n_j^{(g)} + \sum_{j=1}^{s}n_j^{(g)}\frac{\mu_j^{(g)}}{RT}\right] \tag{17}$$

After the above transformations, the number of variables reduces from $s + \epsilon + 1$ to $\epsilon + 1$, which is favorable when a large amount of species are to be tracked simultaneously. It can be readily verified that the algorithm reduces to the standard NASA CEA one when there is no adsorption, or $r_j = 0$ (for $j = 1, ..., s$).[4]

The procedure of the calculation is to calculate the terms on the right hand side of Eqs. 16 and 17 with initial guesses of $n_j^{(g)}$ and $n_T^{(g)}$, and then solve $\Delta \ln n_T^{(g)}$ and π_k ($k = 1, ..., \epsilon$) using these $\epsilon + 1$ linear equations. Subsequently, $\Delta \ln n_j^{(g)}$ ($j = 1, ..., s$) are calculated using Eq. 13 based on the value of $\Delta \ln n_T^{(g)}$. The following formulas

$$\begin{aligned} \left(n_j^{(g)}\right)^{(m+1)} &= \exp\left[\left(\ln n_j^{(g)}\right)^{(m)} + \alpha^{(m)}\Delta(\ln n_j^{(g)})^{(m)}\right] \qquad (j = 1, ..., s) \\ \left(n_T^{(g)}\right)^{(m+1)} &= \exp\left[\left(\ln n_T^{(g)}\right)^{(m)} + \alpha^{(m)}\Delta(\ln n_T^{(g)})^{(m)}\right] \end{aligned} \tag{18}$$

are then applied to update $n_j^{(g)}$ and $n_T^{(g)}$ to be used in the next iteration step. When the composition is far from equilibrium, a positive α that is smaller than one should be chosen to avoid divergence. When it is close to equilibrium, α is set to be 1. The readers may refer to the NASA CEA technical report[4] for more detailed discussions.

In the above equations, the thermodynamic data of each species at temperature T, such as the heat capacity, enthalpy, entropy and chemical potential are calculated as functions of temperature:[4]

$$\begin{aligned} \frac{c_p^0(T)}{R} &= \frac{a_1}{T^2} + \frac{a_2}{T} + a_3 + a_4 T + a_5 T^2 + a_6 T^3 + a_7 T^4 \\ \frac{H^0(T)}{RT} &= -\frac{a_1}{T^2} + \frac{a_2}{T}\ln T + a_3 + \frac{a_4}{2}T + \frac{a_5}{3}T^2 + \frac{a_6}{4}T^3 + \frac{a_7}{5}T^4 + \frac{a_8}{T} \\ \frac{S^0(T)}{R} &= -\frac{a_1}{2T^2} - \frac{a_2}{T} + a_3 \ln T + a_4 T + \frac{a_5}{2}T^2 + \frac{a_6}{3}T^3 + \frac{a_7}{4}T^4 + a_9 \\ \frac{\mu^{0(g)}}{RT} &= \frac{H^0(T)}{RT} - \frac{S^0(T)}{R} \end{aligned} \tag{19}$$

where $a_1, \ldots, a_9$ are constant for a given species.

Remark 1: Regarding the assumptions made in the problem formulation, if the ideal gas law is not adequately accurate (e.g., under very high system pressures), the partial pressure should be replaced by fugacity when the chemical potential is calculated. The formation of condensed species (e.g., the formation of carbon under low steam/ethanol ratios) is not accounted for in the current work and a more comprehensive algorithm is being developed to have this capability.

Remark 2: When the Gibbs minimization problem is solved using the lagrange multiplier method, only the first-order (necessary) optimality conditions are used. At an optimal solution $n_j^{(g)}$ such that $\frac{\partial f}{\partial n_j^{(g)}} = 0$ ($j = 1, ..., s$), it can be verified that $\frac{\partial^2 f}{\partial {n_j^{(g)}}^2} = RT(1 + r_j)\left(\frac{1}{n_j^{(g)}} - \frac{1}{n_T^{(g)}}\right) > 0$ ($j = 1, ..., s$). Given this fact, the computed optimal solution is indeed a local minimum. Interested readers are directed to open literature for global optimization techniques in the calculation of liquid-gas phase and chemical equilibriums with possible multiple minima and maxima in the Gibbs free energy.[39]

In the solution procedure, the initial estimate of $n_T^{(g)}$ is set to be 0.1 and those of $n_j^{(g)}$ are set to be uniformly distributed. This initial guess corresponds to an average molecular weight of 10, which follows the NASA CEA algorithm.[4] With these estimates, the optimization converges successfully within a small number of iterations in all cases studied in this work.

3 Chemical equilibrium calculation using the equilibrium constant method

Different from the Gibbs minimization method presented in the previous section, the Gibbs energy of the adsorbed species is not required if the amount ratios r_j are available. However, a set of gaseous reactions should be specified before the concept of equilibrium constant can be applied. A reaction scheme can be determined using a set of independent reactions such that any gaseous reaction in this reactive system can be expressed by a linear sum of these basis reactions.[40] The minimum number of independent chemical reactions in a reactive system is equal to the number of species minus the rank of the atomic matrix, provided that the former is greater than the latter.[37] For example, if the rank of the atomic matrix is e, the number of independent reactions is $s-e$. In most cases $e=\epsilon$. Occasionally $e<\epsilon$ when not all the row vectors in the atomic matrix are independent.

Consider a small change in the Gibbs free energy in the gaseous phase under isothermal and isobaric conditions:

$$\delta G^{(g)} \quad = \quad \sum_{j=1}^{s} \mu_j^{(g)} \delta n_j^{(g)} \quad = \quad \sum_{j=1}^{s} \mu_j^{(g)} \sum_{i=1}^{s-e} \nu_{ij} \delta \xi_i \tag{20}$$

where ν_{ij} is the stoichiometric coefficient of species j and ξ_i is the reaction extent in the i-th reaction, $\delta G^{(g)}=0$ for any $\delta\xi_i$ at chemical equilibrium implies:

$$\sum_{j=1}^{s} \mu_j^{(g)} \nu_{ij} \quad = \quad 0 \qquad (i=1,...,s-e) \tag{21}$$

A combination of Eqs. 3 and 21 yields:

$$\sum_{j=1}^{s} \nu_{ij} \left[\frac{\mu_j^{0(g)}}{RT} + \ln \frac{P}{P^0} + \ln \frac{n_j^{(g)}}{n_T^{(g)}} \right] \quad = \quad 0 \qquad (i=1,...,s-e) \tag{22}$$

or

$$\prod_{j=1}^{s} \left[\frac{P n_j^{(g)}}{P^0 n_T^{(g)}} \right]^{\nu_{ij}} \quad = \quad \exp\left[\sum_{j=1}^{s} \left(-\nu_{ij} \frac{\mu_j^{0(g)}}{RT} \right) \right] \quad = \quad K_{p_i} \qquad (i=1,...,s-e) \tag{23}$$

which is just the so-called equilibrium constant method.[1]

The Newton-Raphson iterative formula for Eq. 22 is:

$$\sum_{j=1}^{s} \nu_{ij} \Delta \ln n_j^{(g)} - \left(\sum_{j=1}^{s} \nu_{ij} \right) \Delta \ln n_T \quad = \quad -\sum_{j=1}^{s} \nu_{ij} \frac{\mu_j^{(g)}}{RT} \qquad (i=1,...,s-e) \tag{24}$$

As a result, the chemical equilibrium can be solved based on Eqs. 14, 15 and 24 (Note that the effective number of equations in Eqs. 14 is e if $e < \epsilon$. Therefore, the number of variables is equal to the number of equations). The iterative variables are $\Delta \ln n_j^{(g)}$ $(j = 1, ..., s)$ and $\Delta \ln n_T^{(g)}$. Even though more iterative variables are involved in the equilibrium constant method, a solution procedure similar to the one presented in section 2 can be followed.

4 A case study - steam reforming of ethanol with simultaneous CO_2 adsorption

A reactive system consisting of steam and ethanol is studied in this section. The steam reforming of biomass-generated ethanol would be a potentially viable and renewable process for hydrogen production.[29,41,42] Experimental studies have shown that for a system of hydrocarbon (e.g., methane, methanol or ethanol) and steam, the yield and purity of hydrogen can be significantly improved if CO_2 is adsorbed.[31,32,43–46] Calculations in this section will provide a quantitative analysis of the underlying physicochemical behavior.

In this reactive system, $T = 500$ °C and $P = 5$ bar and the feed ratio of C_2H_5OH to H_2O is 1/3, which are from open literature.[47] The species to be tracked in the systems are CH_4, CO, CO_2, C_2H_4, C_2H_5OH, CH_3CHO, H_2, H_2O and O_2. The formation of byproducts such as C_2H_4, CH_3CHO and CH_4 has been observed in the ethanol reforming processes under certain conditions.[29,47] However, only CH_4 is shown to have a differentiable concentration under the operating conditions in this work. CO_2 is assumed to be the only species that is adsorbed on the surface (i.e., only r_{CO_2} can be a nonzero number) even though the adsorption of multiple species can be readily handled with little extra computational effort. A list of the thermodynamic coefficients, the atomic matrix, and the reaction stoichiometric coefficient matrix are shown in Tables 1, 2 and 3 respectively. Note that the reaction scheme is required only in the equilibrium constant method. In Table 3, a set of 6 independent reactions are representative of the entire system because the number of species is 9 and the rank of the atomic matrix is 3.

The conversion rate of ethanol to hydrogen with simultaneous CO_2 adsorption is solved using the algorithms presented in sections 2 and 3. Computer simulations demonstrate that both algorithms end up with the same results. Typically, it takes only seconds to finish hundreds of simulations. For steam reforming of ethanol, the ideal overall reaction would be $C_2H_5OH + 3\ H_2O = 6\ H_2 + 2\ CO_2$, which corresponds to a 100% conversion of C_2H_5OH to H_2. When CO_2 is adsorbed under different $CO_2^{(ads)}/CO_2^{(g)}$ ratios, the H_2 yield is shown in Figure 1. Note that the horizontal axis is chosen to be $r_{CO_2} = CO_2^{(ads)}/CO_2^{(g)}$ instead of $CO_2^{(ads)}$ because the former is roughly proportional to the amount of adsorbent, and therefore, the size of the reactor (See Figure 2 for a plot generated based on Eq. 5 and the results from the equilibrium calculation. β_{CO_2} under the operating conditions in this work is estimated to be 22 bar^{-1} based on the experimental data of promoted hydrotalcites[48]). It is seen that with no or little CO_2 adsorption, the conversion rate of C_2H_5OH to H_2 is only 15.4%, which is consistent with the NASA CEA code.[4] When CO_2 is adsorbed, the conversion can be significantly enhanced. For example, at $CO_2^{(ads)}/CO_2^{(g)} = 10^2$, the conversion rate of C_2H_5OH to H_2 is 38.9%, or enhanced by a factor greater than 2 (A list of the composition under these two conditions is shown in Table 4). However, a further improvement in the conversion of C_2H_5OH to H_2 requires a significant increase in $CO_2^{(ads)}/CO_2^{(g)}$, or the amount of adsorbent. This can be explained by Figure 3, in which it is shown that as CO_2 is adsorbed on the surface, a further removal of CO_2 from the gas phase becomes more and more difficult.

The gas composition in the product mixture under different $CO_2^{(ads)}/CO_2^{(g)}$ ratios is shown in Figure 4. Under the operating conditions of interest, none of C_2H_4, CH_3CHO, C_2H_5OH or O_2 has a differentiable fraction in the product mixture. As $CO_2^{(ads)}/CO_2^{(g)}$ increases, the fraction of $CO_2^{(g)}$ rapidly decreases to a minimal level (at $CO_2^{(ads)}/CO_2^{(g)} = 10^{1\sim2}$), beyond which a significant reduction in the $CO_2^{(g)}$ concentration is not obvious. The low partial pressure of CO_2 in the gas phase makes it difficult for an effective adsorption. In fact, at $CO_2^{(ads)}/CO_2^{(g)} > 10^1$ the primary carrier of carbon in the gaseous phase is CH_4 instead of CO or CO_2. When CO_2 is gradually adsorbed on the surface, the forward reaction in the reversible water gas shift reaction $CO + H_2O = CO_2 + H_2$ is favored. As a result, part of the CH_4 is converted to CO through the methane reforming reaction $CH_4 + H_2O = CO + 3\ H_2$. In this sense, the entire system behaves like a buffer solution. Due to the coupling of multiple equilibrium phenomena, a complete removal of CO_2 is very difficult.

An interesting phenomenon is also observed in this reactive system regarding the specific volume of the product mixture. Note that the calculation is based on a fixed amount of mass (i.e., 1 kilogram) of the reactant mixture, and therefore, the volume of the product is proportional to the total amount $n_T^{(g)}$. As shown in Figure 5, the volume of the gas mixture expands about 1.37 times at equilibrium if there is no CO_2 adsorption. According to Le Chatelier's principle, a low system pressure is preferred for a high conversion of C_2H_5OH to H_2 at chemical equilibrium, which is consistent with experimental observations.[47] When CO_2 is gradually adsorbed on the surface, the volume of the product shrinks. After reaching a minimum at a $CO_2^{(ads)}/CO_2^{(g)}$ ratio around 14, the volume of the product increases even as CO_2 is adsorbed. This is because the effect of volume expansion due to methane reforming $CH_4 + H_2O = CO + 3\ H_2$ is greater than the shrinking effect caused by CO_2 adsorption.

Figure 6 shows the relationship between the conversion rate of C_2H_5OH to H_2 as a function of the CO_2 removal ratio, defined as the absolute amount of CO_2 adsorbed on the surface divided by its theoretical upper limit. It is seen that the enhancement in the H_2 production is not significant when the CO_2 removal ratio is below 40% (corresponding to a $CO_2^{(ads)}/CO_2^{(g)}$ around 13). This is because the methane reforming reaction and the water gas shift reaction shift only a little to the right, which is reflected by the fact that the total amount drops significantly (see Figure 5) and that the fraction of CH_4 and H_2O might even increase (see the peaks in CH_4 and H_2O fractions in Figure 4). As the CO_2 removal ratio exceeds 40%, the H_2 production increases linearly (A similar phenomenon is observed in H_2 purity). In such a case, there is little CO_2 or CO in the gas phase (Figure 4), and therefore, the overall reaction in the gas phase is $CH_4 + 2\ H_2O = CO_2 + 4\ H_2$. Because the CO_2 generation rate is roughly balanced by its adsorption rate, 4 mole of H_2 will be generated when 1 mole of CO_2 is removed from the gas phase by adsorption. If the result is interpreted in terms of the H_2 production and CO_2 removal ratio, the slope is 4/3 because the ideal reaction is $C_2H_5OH + 3\ H_2O = 6\ H_2 + 2\ CO_2$.

The reactive system in the above analysis is based on a setting similar to a single stage batch reactor, in which the gas phase has a uniform composition and is in equilibrium with the adsorbent. If a reforming reactor is divided into several zones (or stages) and a local chemical equilibrium is maintained in each zone, the overall hydrogen yield at the end of the reactor could be higher. This is because CO_2, once being adsorbed on the surface, does not have an effect on the reactive system downstream, which is true in a real reforming reactor. In the next case study, the CO_2 is adsorbed using multiple stages in series. This is realized by setting the gas composition at the outlet of one stage to be the inlet composition at the next stage. In addition, the gaseous reactive system at each stage is in local equilibrium with the adsorbent. Four cases are studied in which the stage $CO_2^{(ads)}/CO_2^{(g)}$ ratios are different. However, the product of $CO_2^{(ads)}/CO_2^{(g)}$ and the number of stages is fixed which makes the total adsorbent area roughly the same. A smaller $CO_2^{(ads)}/CO_2^{(g)}$ at each equilibrium stage corresponds to a shorter time scale for reaction and adsorption equilibrium. In each case, the cumulative adsorbent surface area and the H_2 yield are solved as functions of number of stages times $CO_2^{(ads)}/CO_2^{(g)}$ and the results are shown in Figures 7 and 8. It is seen that the cumulative adsorbent surface area is a linear function of the number of stages and the total surface areas are indeed roughly the same in all cases. However, the conversion rate to hydrogen might be higher if the reaction and adsorption equilibrium are faster, even though the difference becomes smaller at an adequately large adsorbent area. In all cases, the long tails in the hydrogen yield profiles suggest that an improvement in the hydrogen yield becomes more and more challenging and a trade off between the adsorbent size and the hydrogen yield should be made.

Based on this finding, and the fact that the overall gas phase reaction is endothermic at high hydrogen yields, an integrated process design could encompass the heat exchange between the endothermic reforming and exothermic combustion of remaining CO and CH_4 in the off-gas downstream of a H_2 separation unit. See Figure 9 for a schematic of this process. C_2H_5OH and H_2O are preheated by the flue gas before entering the reformer, where H_2 is generated and a major part of CO_2 is adsorbed. The product mixture passes through a hydrogen separation unit (e.g., a pressure swing adsorption unit, or PSA), where H_2 is separated from unconverted CH_4, H_2O as well as some CO and CO_2 in trace amount. The CH_4 from the H_2 separation unit is sent to a combustor where heat is supplied to the reformer as well as the feed streams (C_2H_5OH and H_2O) through heat exchange (HE) units. Interested readers might find more discussions in autothermal processes in open literature.[24,29,49–51] If the heat released from the CO_2 adsorption is not taken into account (since it will be released in subsequent CO_2 desorption), a plot of the heat demand in the reformer and the heat supply in the combustor v.s. the CO_2 removal ratio is given in Figure 10. Under the current operating conditions, the gaseous reaction could be exothermic (i.e., negative heat demand) at low CO_2 removal ratios where the H_2 yields are also low (see Figure 6). However, as the H_2 yield increases, the reforming reaction becomes endothermic and the waste heat provided by the combustion of un-reacted CH_4 and CO decreases. A heat neutral point occurs at a CO_2 removal ratio around 90%. In the above calculation both reactions occur at 500 °C. Therefore, it does not account for pre-heating of feed streams to 500 °C or cooling of flue gases to room temperature or the energy required for the H_2 separation unit. Moreover, a 100% efficiency of heat transfer between these two processes is assumed. This rough calculation indicates that an 86.3% theoretical maximum overall conversion of C_2H_5OH to H_2 (the corresponding H_2 purity in the product mixture out of the reformer is 89.4% on wet basis or 96.2% on dry basis, see Table 5 for the composition of other components.) can be achieved with little or no external heat supply in the reforming process if combined with simultaneous CO_2 adsorption. The reactions in the reformer reactor and the combustor as well as the overall reaction of the entire process (T = 500 °C) are summarized as follows:

$$\begin{array}{lrcl}
\text{(1)} & C_2H_5OH + 3\ H_2O & = & 0.2052\ CH_4 + 5.1790\ H_2 + 0.4105\ H_2O + 1.7947\ CO_2\ \text{(ads)} \\
\text{(2)} & 0.2052\ CH_4 + 0.4105\ O_2 & = & 0.2052\ CO_2 + 0.4105\ H_2O \\
\hline
\text{(sum)} & C_2H_5OH + 3\ H_2O + 0.4105\ O_2 & = & 0.2052\ CO_2 + 5.1790\ H_2 + 0.8210\ H_2O + 1.7947\ CO_2\ \text{(ads)}
\end{array}$$

Note that the gaseous CO and CO_2 in trace amount are not listed above. The net energy demand of the combined reforming and combustion process is zero at 500 °C if the heat released from CO_2 adsorption is not taken into account ($\Delta H_1 = -\Delta H_2 = 1.64 \times 10^5$ J/mol. In Figure 10 the heat demand and supply are both 1.64×10^6 J because they are based on 1 kilogram of the ethanol and steam mixture, which contains 10 moles of ethanol and 30 moles of steam). The overall H_2 yield could be less if the heat transfer efficiency and the operating cost are taking into account in this integrated process. A more detailed engineering calculation, which includes regeneration of CO_2, will be presented in a separate work.

It should be noted that even though the equilibrium calculation can provide a mean-field analysis and predict the overall trend of a reforming process, it is not adequate to mimic the real operation. Due to the continuous nature of the adsorption enhanced reforming process, a full description requires kinetic models (including the kinetics of reactions and adsorption/desorption as well). Interested readers are directed to open literature[30,32] for research efforts in this direction.

5 Concluding remarks

Two approaches for the calculation of chemical equilibrium in a gaseous reactive system combined with simultaneous species adsorption are developed in this work following algorithms similar to the NASA CEA code. Both algorithms are very effective in solving gaseous reactive systems with simultaneous species adsorption. Whereas the equilibrium constant method requires specifying a set of independent reactions and solving more nonlinear equations, these reactions are useful in the analysis of various coupled equilibrium phenomena in the entire reactive system.

The algorithms are applied to an enhanced ethanol reforming system where CO_2 is partially or fully removed by adsorption. It is shown that at T = 500 °C and P = 5 bar, the CO_2 removal ratio should exceed 40% in order to achieve a decent enhancement in hydrogen production and purity. Whereas the hydrogen production increases linearly with the CO_2 removal ratio if the latter is higher than 40%, the amount of adsorbent (and therefore, the reactor size) required for CO_2 increases exponentially. A trade off between the H_2 production and the reactor size can be achieved by burning CH_4 in the off-gas from the H_2 separation unit to provide heat for the endothermic reforming process. It is shown that a theoretical maximum overall conversion of C_2H_5OH to H_2 around 86.3% can be achieved with little or no external heat supply in the reforming process if combined with simultaneous CO_2 adsorption (the corresponding H_2 purity in the product mixture out of the reformer is 89.4% on wet basis or 96.2% on dry basis).

Even though the adsorption of a single species is discussed in the case study, the algorithms can be potentially applied to multiple species adsorption in a similar manner.

Acknowledgements

This work is partly supported by Intelligent Energy, Inc. (through a DOE subcontract) and the Faculty Center for Professional Development at California State Polytechnic University, Pomona. Industrial feedback from Dr. Durai Swamy and coworkers at Intelligent Energy, Long Beach, CA and discussions with Drs. T. K. Nguyen and W. Dong are gratefully acknowledged.

References

1. Sandler, S. I. *Chemical and Engineering Thermodynamics*, 3rd ed.; Wiley: New York, 1999.

2. Huzel, D. K.; Huang, D. H. *Design of Liquid Propellant Rocket Engines*; Technical Report NASA SP-125, 1971.

3. Tran, D. H.; Snyder, C. A. *Effects of Chemical Equilibrium on Turbine Engine Performance for Various Fuels and Combustor Temperatures*; Technical Report NASA TM-105399, 1992.

4. Gordon, S.; McBride, B. J. *Computer Program for Calculation of Complex Chemical Equilibrium Compositions and Applications*; Technical Report NASA RP-1311, 1996.

5. Hysys 4.0 User Guide; Aspen Technology, Inc., 2004.

6. Pro/II 8.0 User Guide; Invensys Systems, Inc., 2006.

7. Rao, Y. K. Chemical vapour deposition of WSi_2 thin films: Equilibrium W-Si-H-Cl-Ar system. *J. Alloys Compd.* **2008**, *452*, 116–121.

8. Won, Y. S.; Varanasi, V. G.; Kryliouk, O.; Anderson, T. J.; McElwee-White, L.; Perez, R. J. Equilibrium analysis of zirconium carbide CVD growth. *J. Cryst. Growth* **2007**, *307*, 302–308.

9. Lay-Son, M.; Drakides, C. New approach to optimize operational conditions for the biological treatment of a high-strength thiocyanate and ammonium waste: pH as key factor. *Water Res.* **2008**, *42*, 774–780.

10. Smirnov, V. V.; Brinkley, D. W.; Lanci, M. P.; Karlin, K. D.; Roth, J. P. Probing metal-mediated O_2 activation in chemical and biological systems. *J. Mol. Catal. A: Chem.* **2006**, *251*, 100–107.

11. Li, M.; Christofides, P. D. Multi-scale Modeling and Analysis of HVOF Thermal Spray Process. *Chem. Eng. Sci.* **2005**, *60*, 3649–3669.

12. Li, M.; Shi, D.; Christofides, P. D. Diamond Jet Hybrid HVOF Thermal Spray: Gas-phase and Particle Behavior Modeling and Feedback Control Design. *Ind. Eng. Chem. Res.* **2004**, *43*, 3632–3652.

13. Li, M.; Christofides, P. D. Computational study of particle in-flight behavior in the HVOF thermal spray process. *Chem. Eng. Sci.* **2006**, *61*, 6540–6552.

14. Li, M.; Christofides, P. D. Modeling and Analysis of HVOF Thermal Spray Process Accounting for Powder Size Distribution. *Chem. Eng. Sci.* **2003**, *58*, 849–857.

15. Assabumrungrat, S.; Laosiripojana, N.; Pavarajarn, V.; Sangtongkitcharoen, W.; Tangjitmatee, A.; Praserthdam, P. Thermodynamic analysis of carbon formation in a solid oxide fuel cell with a direct internal reformer fuelled by methanol. *J. Power Sources* **2005**, *139*, 55–60.

16. Assabumrungrat, S.; Pavarajarn, V.; Charojrochkul, S.; Laosiripojana, N. Thermodynamic analysis for a solid oxide fuel cell with direct internal reforming fueled by ethanol. *Chem. Eng. Sci.* **2004**, *59*, 6015–6020.

17. Colpan, C. O.; Dincer, I.; Hamdullahpur, F. Thermodynamic modeling of direct internal reforming solid oxide fuel cells operating with syngas. *Int. J. Hydrogen Energy* **2007**, *32*, 787–795.

18. Ding, Y.; Alpay, E. Equilibria and kinetics of CO_2 adsorption on hydrotalcite adsorbent. *Chem. Eng. Sci.* **2000**, *55*, 3461–3474.

19. Lutz, A. E.; Bradshaw, R. W.; Bromberg, L.; Rabinovich, A. Thermodynamic analysis of hydrogen production by partial oxidation reforming. *Int. J. Hydrogen Energy* **2004**, *29*, 809–816.

20. Lutz, A. E.; Bradshaw, R. W.; Keller, J. O.; Witmer, D. E. Thermodynamic analysis of hydrogen production by steam reforming. *Int. J. Hydrogen Energy* **2003**, *28*, 159–167.

21. Matelli, J. A.; Bazzo, E. A methodology for thermodynamic simulation of high temperature, internal reforming fuel cell systems. *J. Power Sources* **2005**, *142*, 160–168.

22. Nikulshina, V.; Hirsch, D.; Mazzotti, M.; Steinfeld, A. CO_2 capture from air and co-production of H_2 via the $Ca(OH)_2$-$CaCO_3$ cycle using concentrated solar power-Thermodynamic analysis. *Energy* **2006**, *31*, 1715–1725.

23. Posada, A.; Manousiouthakis, V. Hydrogen and dry ice production through phase equilibrium separation and methane reforming. *J. Power Sources* **2005**, *156*, 480–488.

24. Hershkowitz, F.; Berlowitz, P. J.; Socha, R. F.; Marucchi-Soos, E.; Frederick, J. W. Hydrogen Production via Steam Reforming in a Reverse-Flow Reactor. *Proceedings of AIChE Annual Meeting*, New York, 2005.

25. Sharma, A.; Takanohashi, T.; Morishita, K.; Takarada, T.; Saito, I. Low temperature catalytic steam gasification of HyperCoal to produce H_2 and synthesis gas. *Fuel* **2008**, *87*, 491–497.

26. Gupta, P.; Velazquez-Vargas, L. G.; Li, F.; Fan, L. S. Chemical looping combustion of coal. *Proceedings of AIChE Annual Meeting*, New York, 2005.

27. Steinfeld, A. Solar Thermochemical Production of Hydrogen - A Review. *Sol. Energy* **2005**, *78*, 603–615.

28. Scholz, W. H. Processes for industrial production of hydrogen and associated environmental effects. *Gas Sep. Purif.* **1993**, *7*, 131–139.

29. Deluga, G. A.; Salge, J. R.; Schmidt, L. D.; Verykios, X. E. Renewable Hydrogen from Ethanol by Autothermal Reforming. *Science* **2004**, *303*, 993–997.

30. Ding, Y.; Alpay, E. Adsorption-enhanced steam-methane reforming. *Chem. Eng. Sci.* **2000**, *55*, 3929–3940.

31. Hufton, J. R.; Mayorga, S.; Sircar, S. Sorption-enhanced reaction process for hydrogen production. *AIChE J.* **1999**, *45*, 248–256.

32. Xiu, G.; Li, P.; Rodrigues, A. E. New generalized strategy for improving sorption-enhanced reaction process. *Chem. Eng. Sci.* **2003**, *58*, 3425–3437.

33. Yong, Z.; Mata, V. G.; Rodrigues, A. E. Adsorption of Carbon Dioxide on Chemically Modified High Surface Area Carbon-Based Adsorbents at High Temperature. *Adsorption* **2001**, *7*, 41–50.

34. Lee, K. B.; Beaver, M. G.; Caram, H. S.; Sircar, S. Chemisorption of carbon dioxide on sodium oxide promoted alumina. *AIChE J.* **2007**, *53*, 2824–2831.

35. Lee, K. B.; Beaver, M. G.; Caram, H. S.; Sircar, S. Novel Thermal-Swing Sorption-Enhanced Reaction Process Concept for Hydrogen Production by Low-Temperature Steam-Methane Reforming. *Ind. Eng. Chem. Res.* **2007**, *46*, 5003–5014.

36. Langmuir, I. The adsorption of gases on plain surfaces of glass, mica and platinum. *J. Am. Chem. Soc.* **1918**, *40*, 1361–1403.

37. Li, M. Synthesis of Thermodynamically Feasible Reaction Pathways. *Proceedings of AIChE Annual Meeting*, New York, 2004.

38. Press, W. H.; Teukolsky, S. A.; Vetterling, W. T.; Flannery, B. P. *Numerical recipes in C++: the art of scientific computing*, 2nd ed.; Cambridge University Press: New York, USA, 1997.

39. McDonald, C. M.; Floudas, C. A. Global optimization for the phase and chemical equilibrium problem: application to the NRTL equation. *Comput. Chem. Eng.* **1995**, *19*, 1111–1139.

40. Aris, R.; Mah, R. H. S. Independence of Chemical Reactions. *Ind. Eng. Chem. Fund.* **1963**, *2*, 90–94.

41. Arteaga, L. E.; Peralta, L. M.; Kafarov, V.; Casas, Y.; Gonzales, E. Bioethanol steam reforming for ecological syngas and electricity production using a fuel cell SOFC system. *Chem. Eng. J.* **2008**, *136*, 256–266.

42. Florin, N. H.; Harris, A. T. Enhanced hydrogen production from biomass with in situ carbon dioxide capture using calcium oxide sorbents. *Chem. Eng. Sci.* **2008**, *63*, 287–316.

43. Stevens, J. F.; Krishnamurthy, B.; Atanassova, P.; Spilker, K. *Development of 50 kW Fuel Processor for Stationary Fuel Cell Applications*; DOE Technical Report DOE/GO/13102-1, 2007.

44. Ortiz, A. L.; Harrison, D. P. Hydrogen production using sorption-enhanced reaction. *Ind. Eng. Chem. Res.* **2001**, *40*, 5102–5109.

45. Wang, Y. N.; Rodrigues, A. E. Hydrogen production from steam methane reforming coupled with in situ CO_2 capture: Conceptual parametric study. *Fuel* **2005**, *84*, 1778–1789.

46. Koumpouras, G. C.; Alpay, E.; Stepanek, F. Mathematical modelling of low-temperature hydrogen production with in situ CO_2 capture. *Chem. Eng. Sci.* **2007**, *62*, 2833–2841.

47. Rampe, T.; Hubner, P.; Vogel, B.; Heinzel, A. Hydrogen Generation from Ethanol by Allothermal Reforming. *Proceedings of the First World Conference on Biomass for Energy and Industry*, 2001; pp 1889–1892.

48. Lee, K. B.; Verdooren, A.; Caram, H. S.; Sircar, S. Chemisorption of carbon dioxide on potassium-carbonate-promoted hydrotalcite. *J. Colloid Interface Sci.* **2007**, *308*, 30–39.

49. Baldea, M.; Daoutidis, P. Dynamics and control of autothermal reactors for the production of hydrogen. *Chem. Eng. Sci.* **2007**, *62*, 3218–3230.

50. Tiemersma, T. P.; Patil, C. S.; van Sint Annaland, M.; Kuipers, J. A. M. Modelling of packed bed membrane reactors for autothermal production of ultrapure hydrogen. *Chem. Eng. Sci.* **2006**, *61*, 1602–1616.

51. Iordanidis, A. A.; Kechagiopoulos, P. N.; Voutetakis, S. S.; Lemonidou, A. A.; Vasalos, I. A. Autothermal sorption-enhanced steam reforming of bio-oil/biogas mixture and energy generation by fuel cells: Concept analysis and process simulation. *Int. J. Hydrogen Energy* **2006**, *31*, 1058–1065.

List of Tables

Table 1: Coefficients for thermodynamic properties.[4]

	CH_4	CO	CO_2
a_1	-1.766850998E+05	1.489045326E+04	4.943650540E+04
a_2	2.786181020E+03	-2.922285939E+02	-6.264116010E+02
a_3	-1.202577850E+01	5.724527170E+00	5.301725240E+00
a_4	3.917619290E-02	-8.176235030E-03	2.503813816E-03
a_5	-3.619054430E-05	1.456903469E-05	-2.127308728E-07
a_6	2.026853043E-08	-1.087746302E-08	-7.689988780E-10
a_7	-4.976705490E-12	3.027941827E-12	2.849677801E-13
a_8	-2.331314360E+04	-1.303131878E+04	-4.528198460E+04
a_9	8.904322750E+01	-7.859241350E+00	-7.048279440E+00
	C_2H_4	CH_3CHO	C_2H_5OH
a_1	-1.163605836E+05	-1.373904369E+05	-2.342791392E+05
a_2	2.554851510E+03	2.559937679E+03	4.479180550E+03
a_3	-1.609746428E+01	-1.340470172E+01	-2.744817302E+01
a_4	6.625779320E-02	5.922128620E-02	1.088679162E-01
a_5	-7.885081860E-05	-6.240006050E-05	-1.305309334E-04
a_6	5.125224820E-08	3.703324410E-08	8.437346400E-08
a_7	-1.370340031E-11	-9.342697410E-12	-2.234559017E-11
a_8	-6.176191070E+03	-3.318731310E+04	-5.022229000E+04
a_9	1.093338343E+02	1.007417652E+02	1.764829211E+02
	H_2	H_2O	O_2
a_1	4.078322810E+04	-3.947960830E+04	-3.425563420E+04
a_2	-8.009185450E+02	5.755731020E+02	4.847000970E+02
a_3	8.214701670E+00	9.317826530E-01	1.119010961E+00
a_4	-1.269714360E-02	7.222712860E-03	4.293889240E-03
a_5	1.753604930E-05	-7.342557370E-06	-6.836300520E-07
a_6	-1.202860160E-08	4.955043490E-09	-2.023372700E-09
a_7	3.368093160E-12	-1.336933246E-12	1.039040018E-12
a_8	2.682484380E+03	-3.303974310E+04	-3.391454870E+03
a_9	-3.043788660E+01	1.724205775E+01	1.849699470E+01

Table 2: Atomic matrix.

	CH_4	CO	CO_2	C_2H_4	CH_3CHO	C_2H_5OH	H_2	H_2O	O_2
(C)	1	1	1	2	2	2	0	0	0
(H)	4	0	0	4	4	6	2	2	0
(O)	0	1	2	0	1	1	0	1	2

Table 3: Reaction stoichiometric matrix*.

Reaction No.	CH_4	CO	CO_2	C_2H_4	CH_3CHO	C_2H_5OH	H_2	H_2O	O_2
(1)	1	1	0	0	0	-1	1	0	0
(2)	-1	1	0	0	0	0	3	-1	0
(3)	0	-1	1	0	0	0	1	-1	0
(4)	0	2	-2	0	0	0	0	0	1
(5)	0	0	0	0	1	-1	1	0	0
(6)	-2	0	0	1	0	0	2	0	0

* (used only in the equilibrium constant method)

Table 4: Stoichiometric coefficients of the gas products at equilibrium (the reactants are 1 C_2H_5OH + 3 H_2O).

$CO_2^{(ads)}/CO_2^{(g)}$	CH_4	CO	CO_2	C_2H_4	CH_3CHO	C_2H_5OH	H_2	H_2O	O_2
0	1.2570	0.0489	0.6941	0.0000	0.0000	0.0000	0.9231	2.5629	0.0000
100	0.9773	0.0021	0.0101	0.0000	0.0000	0.0000	2.0888	1.9566	0.0000

Table 5: Product composition under different conditions.

	Post-CO_2 adsorption (wet)	CO_2-H_2O free (dry)
H_2	89.4%	96.2%
CH_4	3.5%	3.8%
H_2O	7.1%	

List of Figures

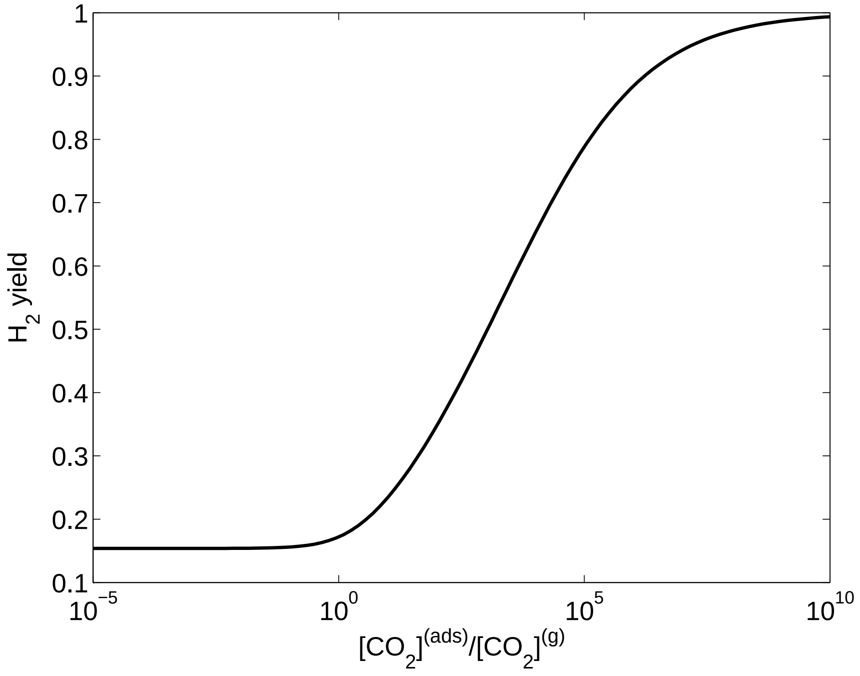

Figure 1: Conversion of C_2H_5OH to H_2 as a function of ${CO_2}^{(\mathrm{ads})}/{CO_2}^{(\mathrm{g})}$ (feed mole ratio = 1/3, P = 5 bar and T = 500 °C).

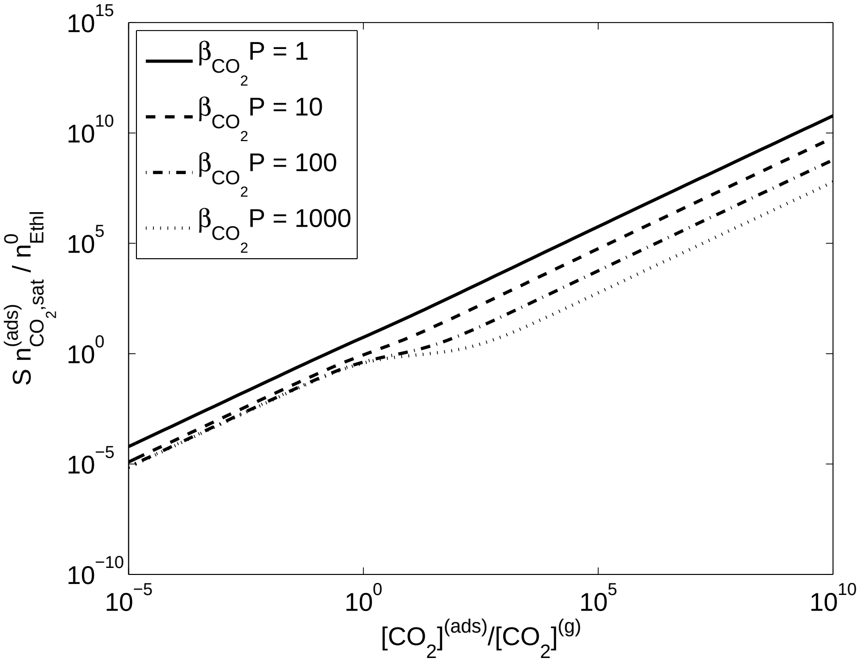

Figure 2: Relationship between ${CO_2}^{(ads)}/{CO_2}^{(g)}$ and the surface area of adsorbent (feed mole ratio = 1/3, $P = 5$ bar and $T = 500$ °C).

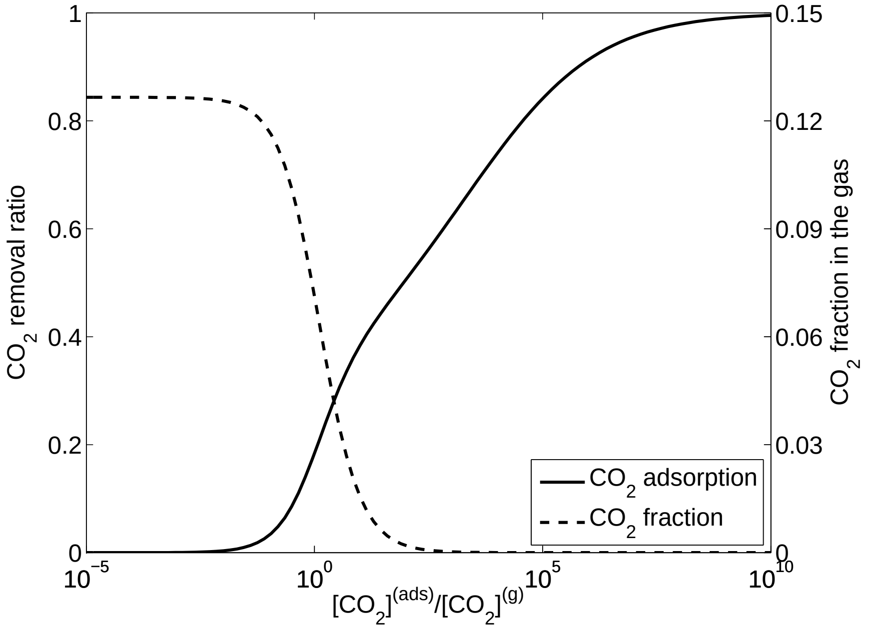

Figure 3: CO_2 removal ratio and CO_2 fraction in the gas as a function of ${CO_2}^{(ads)}/{CO_2}^{(g)}$ (feed mole ratio = 1/3, $P = 5$ bar and $T = 500$ °C).

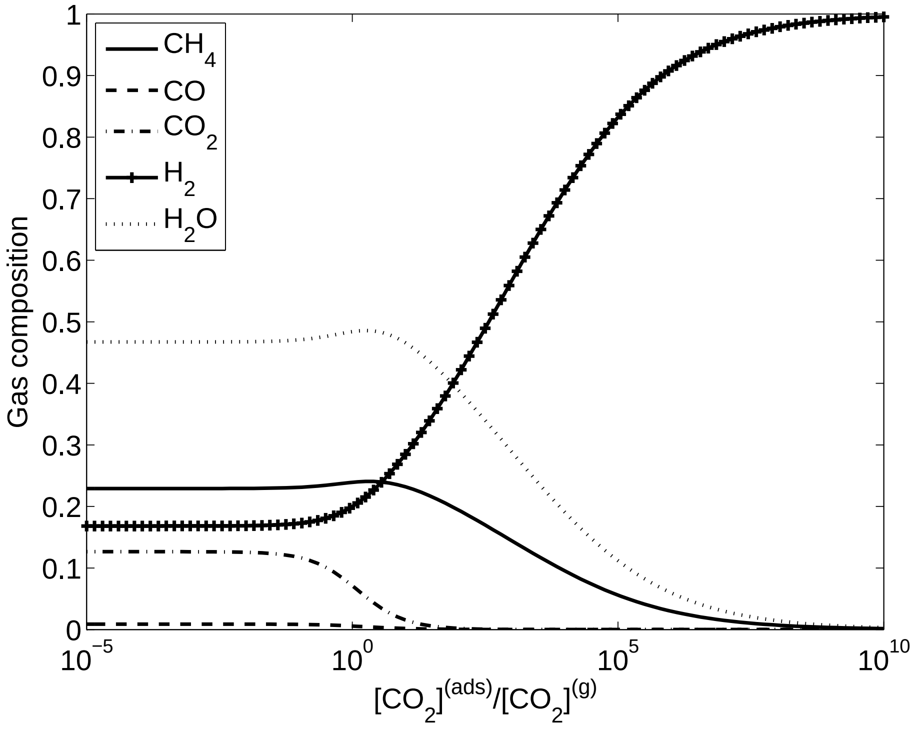

Figure 4: Gas composition at equilibrium as a function of $CO_2{}^{(ads)}/CO_2{}^{(g)}$ (feed mole ratio = 1/3, P = 5 bar and T = 500 °C).

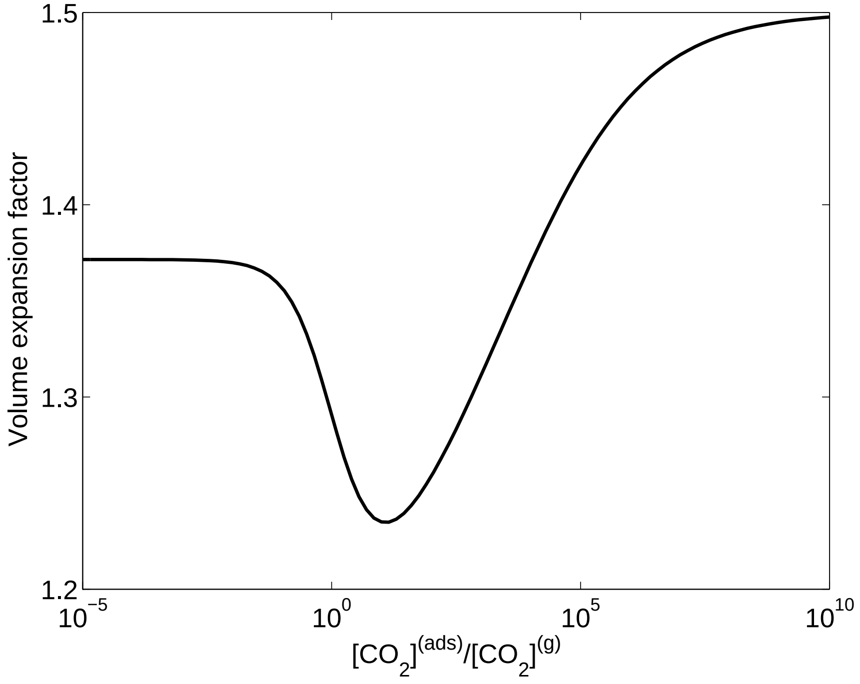

Figure 5: Volume expansion (the volume ratio of the product mixture to the reactant mixture) with respect to the reactant mixture (feed mole ratio = 1/3, $P = 5$ bar and $T = 500$ °C).

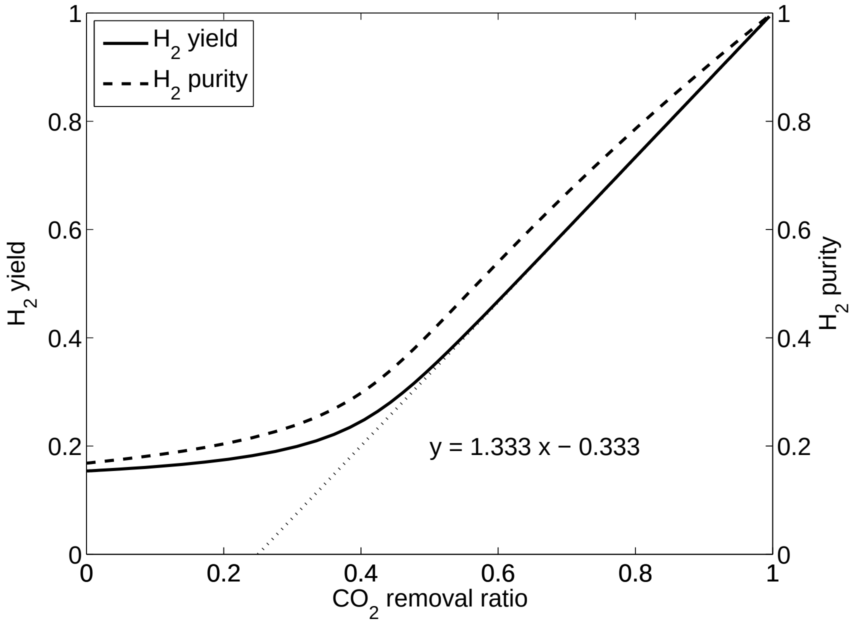

Figure 6: H_2 yield and purity as functions of the CO_2 removal ratio (feed mole ratio = 1/3, $P = 5$ bar and $T = 500$ °C).

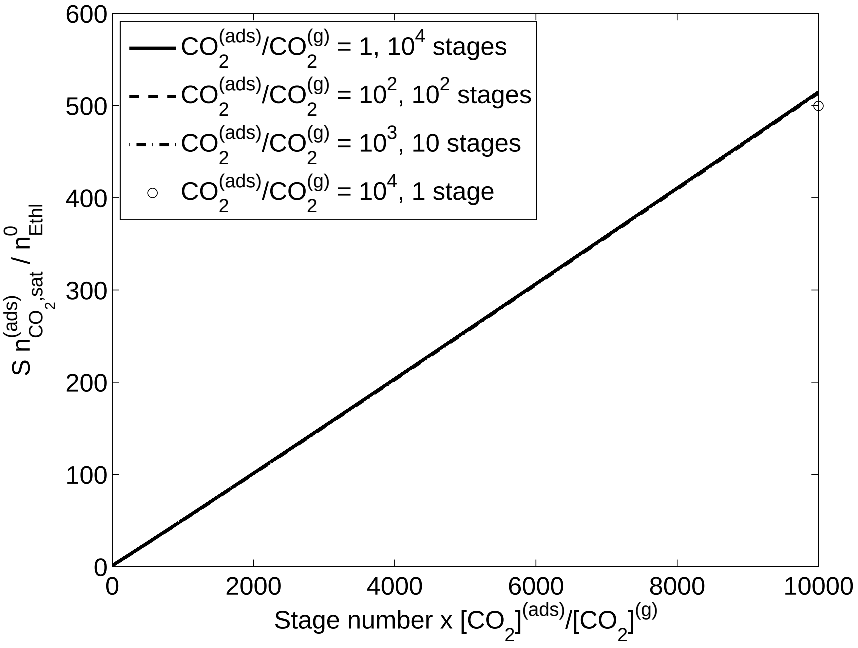

Figure 7: Cumulative adsorbent area as a function of number of equilibrium stages and ${CO_2}^{(ads)}/{CO_2}^{(g)}$ ratios (feed mole ratio = 1/3, $P = 5$ bar and $T = 500$ °C, $\beta_{CO_2} = 22$ bar^{-1}).

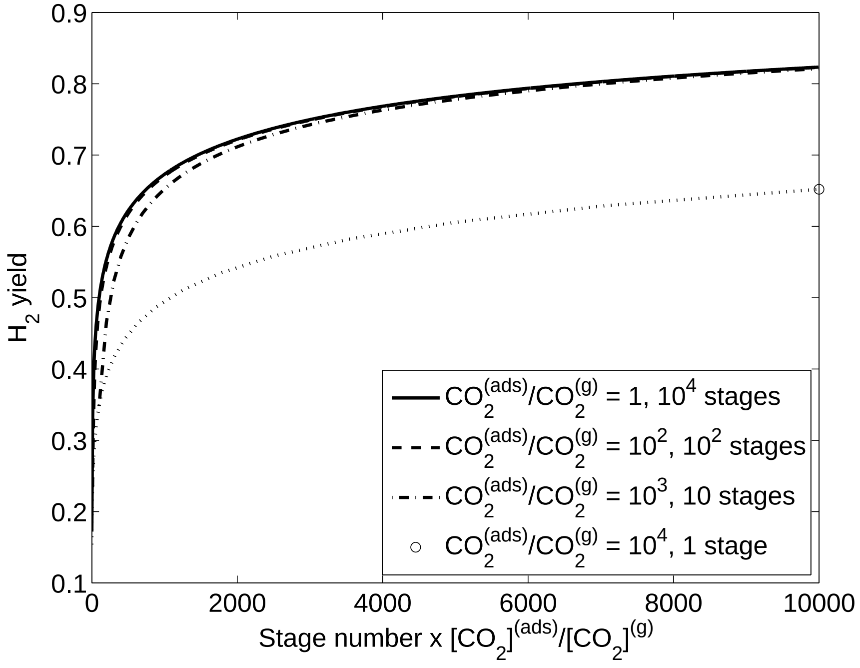

Figure 8: Conversion of C_2H_5OH to H_2 as a function of number of equilibrium stages and ${CO_2}^{(ads)}/{CO_2}^{(g)}$ ratios (feed mole ratio = 1/3, $P = 5$ bar and $T = 500$ °C).

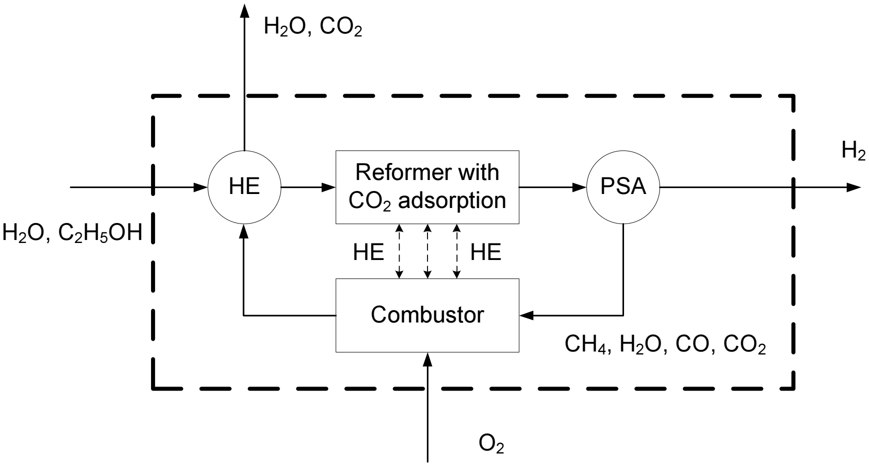

Figure 9: Integrated endothermic reforming and the exothermic combustion of unconverted CH_4 with simultaneous CO_2 in the ethanol reforming process.

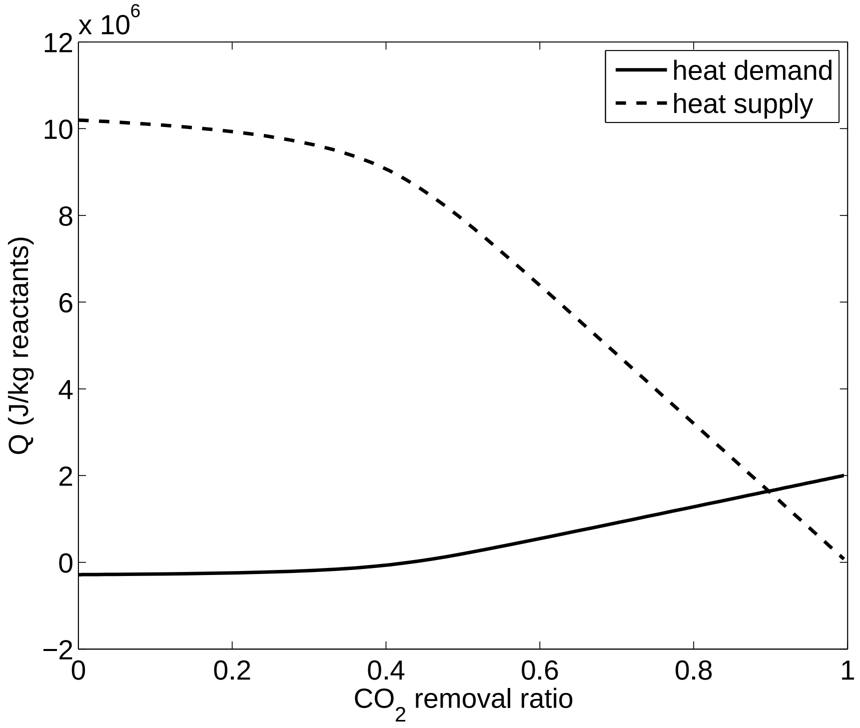

Figure 10: Heat demand by ethanol reforming and heat supply through combustion of exhausting gases from the H_2 separation unit as a function of removal ratio of carbon in the form of CO_2 (feed mole ratio = 1/3, $P = 5$ bar and $T = 500$ °C).